Available online at www.sciencedirect.com
SCIENCE DIRECT®
Quarternary Research 65 (2006) 492–507
QUATERNARY RESEARCH
www.elsevier.com/locate/yqres

Tephrostratigraphy of the Bedded Tuff Member (Kapthurin Formation, Kenya) and the nature of archaeological change in the later middle Pleistocene

Christian A. Tryon [a,b,*], Sally McBrearty [c,1]

[a] *Department of Anthropology, George Washington University, 2110 G St. NW, Washington, DC 20052, USA*
[b] *Human Origins Program, National Museum of Natural History, Smithsonian Institution MS 112, Washington, DC 20560-0112, USA*
[c] *Department of Anthropology, University of Connecticut, Box U-2176, Storrs, CT 06269, USA*

Received 18 November 2004
Available online 10 March 2006

Abstract

Correlation of volcaniclastic deposits of the Bedded Tuff Member (K4) of the Kapthurin Formation (Kenya) provides the means to assess the nature of archaeological change during the later middle Pleistocene, a time period critical to human evolution but poorly represented at other African localities. Field stratigraphic evidence, and petrographic and electron microprobe geochemical analyses of volcanic glass and phenocrysts, define eight subdivisions of K4 tephra. These include a succession of deposits from a local volcanic source that erupted intermittently, as well as other tuffs likely from different sources outside the Baringo basin. Upper portions of the Bedded Tuff Member date to ~235,000 yr. The Bedded Tuff Member is underlain by sediments that include the Grey Tuff, dated to 509,000 ± 9000 yr. The tephrostratigraphic framework defined here is used to place Acheulian and Middle Stone Age (MSA) archaeological sites in chronological order. Results show the persistence of Acheulian large cutting tool manufacture after the advent of points, considered an MSA artifact type. Two assemblages from the site of Koimilot record the appearance at ~200,000–250,000 yr of a variety of Levallois flake production methods, an integral if incompletely understood feature of the MSA, here likely derived from local technological antecedents. Combined evidence from the tools and flake production methods suggest an incremental and mosaic pattern of change in hominin adaptive strategies during the Acheulian–MSA transition.

Keywords: Tephrostratigraphy; Acheulian; Middle Stone Age; Acheulian–MSA transition; Kapthurin Formation; Baringo

Introduction

The later middle Pleistocene in Africa is an important period for understanding the origin of our species. One key archaeological characteristic of this time is the replacement of sites of the Acheulian Industrial Complex by those with diverse Middle Stone Age (MSA) industries (Clark, 1988, 1999; McBrearty, 2001; McBrearty and Brooks, 2000; Tryon and McBrearty, 2002). This change is marked by the disappearance of a long-lived, widespread use of handaxes, cleavers, and knives; their replacement by smaller stone and bone points; and increased emphasis on various Levallois methods of flake production. The earliest sites attributed to the MSA are from the Kapthurin Formation of Kenya and date to >284,000 yr, but Acheulian technology persists until ~160,000 yr in the Middle Awash region of Ethiopia, suggesting that the timing of the Acheulian–MSA transition varied across Africa (Tryon and McBrearty, 2002; Clark et al., 2003). Although defined by differences in lithic technology, MSA sites also differ from those of the Acheulian in ways that may suggest the origin of behavioral modernity at a time when fossil and genetic evidence support the earliest appearance of the *Homo sapiens* lineage (e.g., Lahr and Foley, 1998; Howell, 1999; McBrearty and Brooks, 2000; Stringer, 2002; Tishkoff and Williams, 2002; Henshilwood and Marean, 2003; White et al., 2003; McDougall et al., 2005).

* Corresponding author. Department of Anthropology, George Washington University, 2110 G St. NW, Washington, DC 20052, USA. Fax: +1 202 994 6097.
E-mail addresses: catryon@gwu.edu (C.A. Tryon), mcbrearty@uconn.edu (S. McBrearty).

0033-5894/$ - see front matter © 2006 University of Washington. All rights reserved.
doi:10.1016/j.yqres.2006.01.008

Although no longer the 'muddle in the middle' that it once appeared (Isaac, 1975), the archaeological record remains chronologically poorly resolved for much of the African middle Pleistocene, defined by the onset of the last interglacial and the Matuyama–Brunhes boundary as ~130,000–790,000 yr ago (e.g., Yamei et al., 2000; Singer et al., 2002; Gibbard, 2003; *cf.* Sarna-Wojcicki et al., 2000). Poor chronological resolution limits our understanding of the processes of adaptive change represented by the Acheulian–MSA transition. Two factors may exaggerate differences between Acheulian and MSA sites. First, few locations preserve dated, relatively complete sedimentary and hominin occupational records that span the end of the Acheulian and the advent of the Middle Stone Age. Where MSA strata overlie those of the Acheulian, they are often separated by pronounced unconformities (see Tryon and McBrearty, 2002). Second, most MSA sites are later Pleistocene in age and, at <130,000 yr, substantially postdate the youngest Acheulian sites (Klein, 1999; McBrearty and Brooks, 2000; McBrearty and Tryon, 2006). Clearly, hypotheses regarding the relation between the changes in hominin behavior seen in the archaeological record of the Acheulian–MSA transition, and biological changes seen in the earliest fossil remains of *Homo sapiens*, can proceed only from well-defined temporal frameworks.

We emphasize here data from the Kapthurin Formation of Kenya and detail a stratigraphic framework for a succession of volcanic tephra and archaeological sites that provides the means to assess temporal change across the Acheulian–MSA transition. The Kapthurin Formation joins a limited but growing number of artifact and hominin fossil localities, particularly from eastern Africa, that demonstrate the complexity and diversity of hominin adaptations during the later middle Pleistocene (e.g., Barham, 2000; Clark et al., 2003; Van Peer et al., 2003). Deciphering hominin behavioral adaptations through time must proceed from basic observations of the order of events, achieved here through an integration of archaeological data with tephra correlated by field stratigraphic, petrographic, and geochemical means.

The Kapthurin Formation

Sediments of the Kapthurin Formation crop out west of Lake Baringo in the Kenyan Rift Valley (Figs. 1A and B), are exposed over an area of ~150 km^2, and have a maximum observed thickness of >125 m. Basal Kapthurin Formation sediments unconformably overlie tilted and faulted sediments of the Chemeron Formation (Fig. 1C). Martyn (1969) and Tallon (1976, 1978) divide the volcaniclastic and terrigenous sediments of the Kapthurin Formation into five named and numbered members (Fig. 1C). The Lower, Middle, and Upper Silts and Gravels (K1, K3, and K5, respectively) consist of sediments derived from volcanic highlands in the Tugen Hills (Fig. 1B), deposited in a range of alluvial and lacustrine environments. The Pumice Tuff Member (K2) and the Bedded Tuff Member (K4) separate the three Silts and Gravels members (Fig. 1C). A maximum age for the Kapthurin Formation is provided by a K/Ar date of 1.57 Ma on the Ndau Trachymugearite (Fig. 1C) (Hill et al., 1986). All Kapthurin Formation sediments are normally magnetized (Dagley et al., 1978) and thus postdate the Matuyama–Brunhes boundary, currently estimated at ~790,000 yr (Yamei et al., 2000; Singer et al., 2002; *cf.* Sarna-Wojcicki et al., 2000). As shown in Fig. 1C, a suite of ^{40}Ar/^{39}Ar dates on K2, portions of K4, the discontinuous Grey Tuff, and intercalated lavas provide excellent chronological control for most Kapthurin Formation sediments (Deino and McBrearty, 2002). The termination of Kapthurin Formation sedimentation and the onset of the current erosional regime is defined by a major faulting episode, with U-series age estimates on thermal silica in-filled fault-related cracks on the Lake Baringo Trachyte from ~198,000 to 345,000 yr (Tallon, 1976; Le Gall et al., 2000). This suggests a middle Pleistocene age for all Kapthurin Formation sediments. Sediments unconformably overlying the Kapthurin Formation are of late Pleistocene or Holocene age (Bishop et al., 1971; Renaut and Owen, 1980).

Our focus here is on archaeological sites within the stratigraphic interval bounded by the Grey Tuff, dated to 509,000 ± 9000 yr, and the Bedded Tuff Member, the upper portions of which are dated to 284,000 ± 12,000 yr and 235,000 ± 2000 yr (Deino and McBrearty, 2002) (Fig. 1C). Surface and excavated artifact assemblages from this interval are attributed to the Acheulian, Middle Stone Age, and possibly the Sangoan or Fauresmith industries (Leakey et al., 1969; Cornelissen, 1992, 1995; Cornelissen et al., 1990; McBrearty, 1999, 2001; McBrearty and Tryon, 2006; McBrearty et al., 1996; Tryon, 2002, 2003, in press(a); Tryon and McBrearty, 2002; Tryon et al., in press). Sites are attributed to industry or industrial complex by the presence of diagnostic tool types such as handaxes and points. Kapthurin Formation lithic assemblages are further characterized by a number of different flake production strategies, including widespread opportunistic flaking of locally available lava cobbles, application of various Levallois methods, and rare but significant examples of systematic blade production.

Bedded Tuff Member tephrostratigraphy

The Bedded Tuff Member represents a period of intermittent volcanic activity and tephra deposition into an active depositional environment. The Bedded Tuff Member (K4) consists of airfall and reworked tephra interbedded with predominantly alluvial sediments. At least 15 layers of volcanic ash buried a succession of artifact- and fossil-bearing land surfaces. The stratigraphic ordering of these land surfaces permits observation of temporal change, but variable paleotopography and present outcrop irregularity have resulted in complex patterns of preservation and exposure. The stratigraphic equivalency of tephra deposits among the dispersed outcrops of K4 in which archaeological sites occur is demonstrated by lateral tracing of distinct marker tuffs, petrographic analysis, and geochemical 'fingerprinting' (*cf.* Fisher and Schmincke, 1984; Sarna-Wojcicki and Davis, 1991; Brown, 1994; Feibel, 1999).

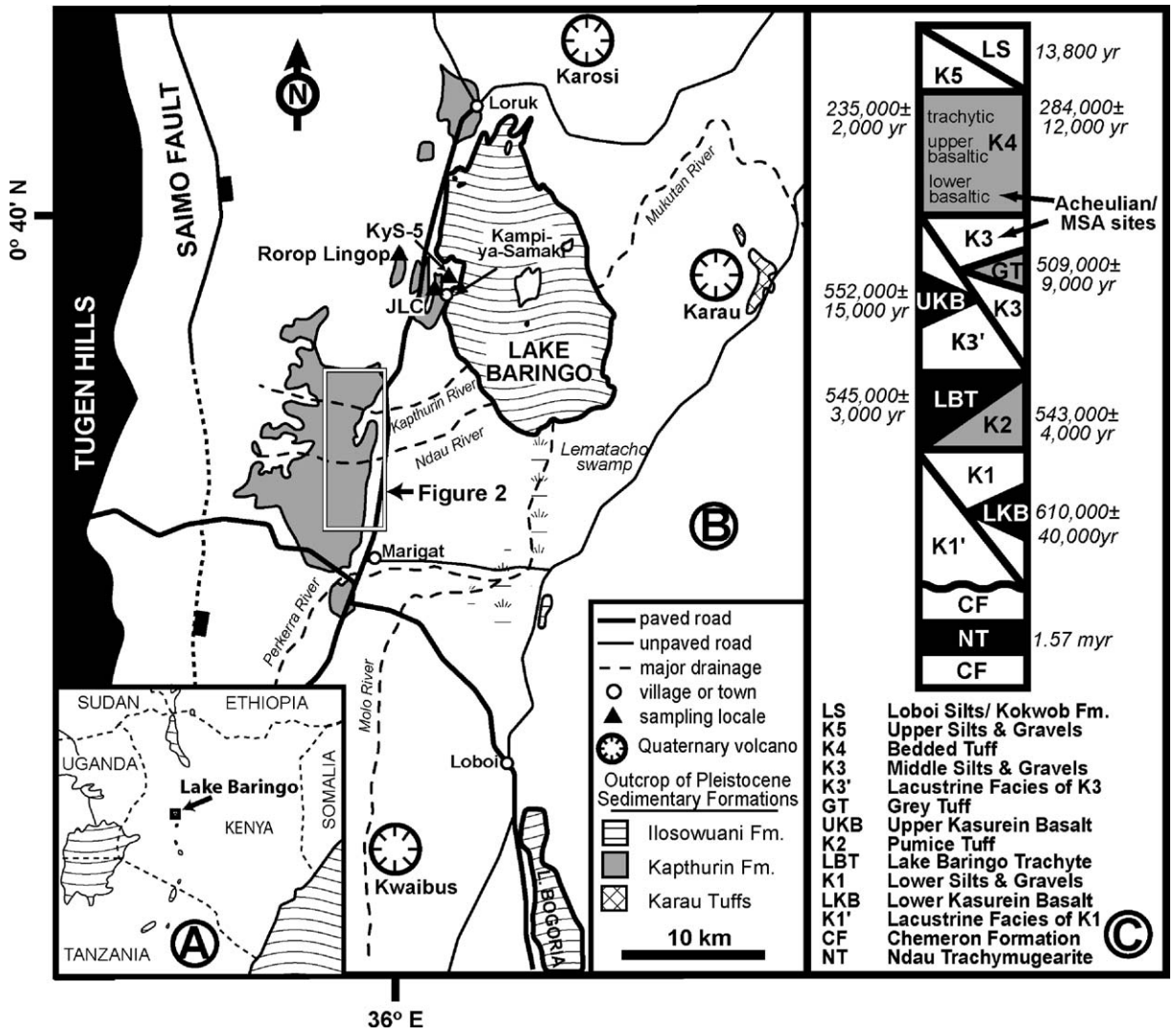

Figure 1. Summary map of the major physiographic features and Pleistocene sediments in the Baringo basin, showing the location of tephra sampling locales discussed in text and the basic stratigraphic succession of the Kapthurin Formation. After Deino and McBrearty (2002) and Tryon and McBrearty (2002); map from Tiercelin et al. (1987) and Chapman et al. (1978).

Previous research on the Bedded Tuff Member (K4) was based on fieldwork conducted from 1997–1999, resulted in the definition of three geochemical subdivisions of K4, and recognized general temporal trends (Tryon and McBrearty, 2002). Results presented here are based on fieldwork in the Baringo area during 2001–2002 and petrographic and geochemical characterization of 27 samples of tephra from 11 new localities that augment and expand prior results. First, a total of eight geochemical and stratigraphic subdivisions are now recognized among Bedded Tuff Member tephra, resulting in increased temporal precision. Second, new areas sampled include those from south of the Kapthurin River and from previously unexplored outcrops south of the Ndau River (Figs. 1B, 2), together providing a broadened geographic scope for tephrostratigraphic correlation within the Kapthurin Formation. Third, these newly explored exposures preserve younger portions of the Bedded Tuff Member sequence and include recently excavated artifacts from the Middle Stone Age site of Koimilot that extends the time span of observed archaeological change.

Archaeological and geological sampling localities

The locations of all tephra sampling localities are shown in Figures 1 and 2. Table 1 provides summary descriptions of these localities and a list of the abbreviations used throughout the text. The available dataset comprises nine archaeological sites with artifacts from surface and excavated contexts from within, above, and beneath tephra deposits of the Bedded Tuff Member. All are open-air sites, and most have relatively low artifact densities and assemblage totals. In all cases, Acheulian and Middle Stone Age shaped tools form a small but typologically significant portion of each assemblage (Table 1). This rarity may be a result of differential preservation and recovery during excavation, the influence of sample size on typological richness (Grayson and Cole, 1998), and past environmental or functional

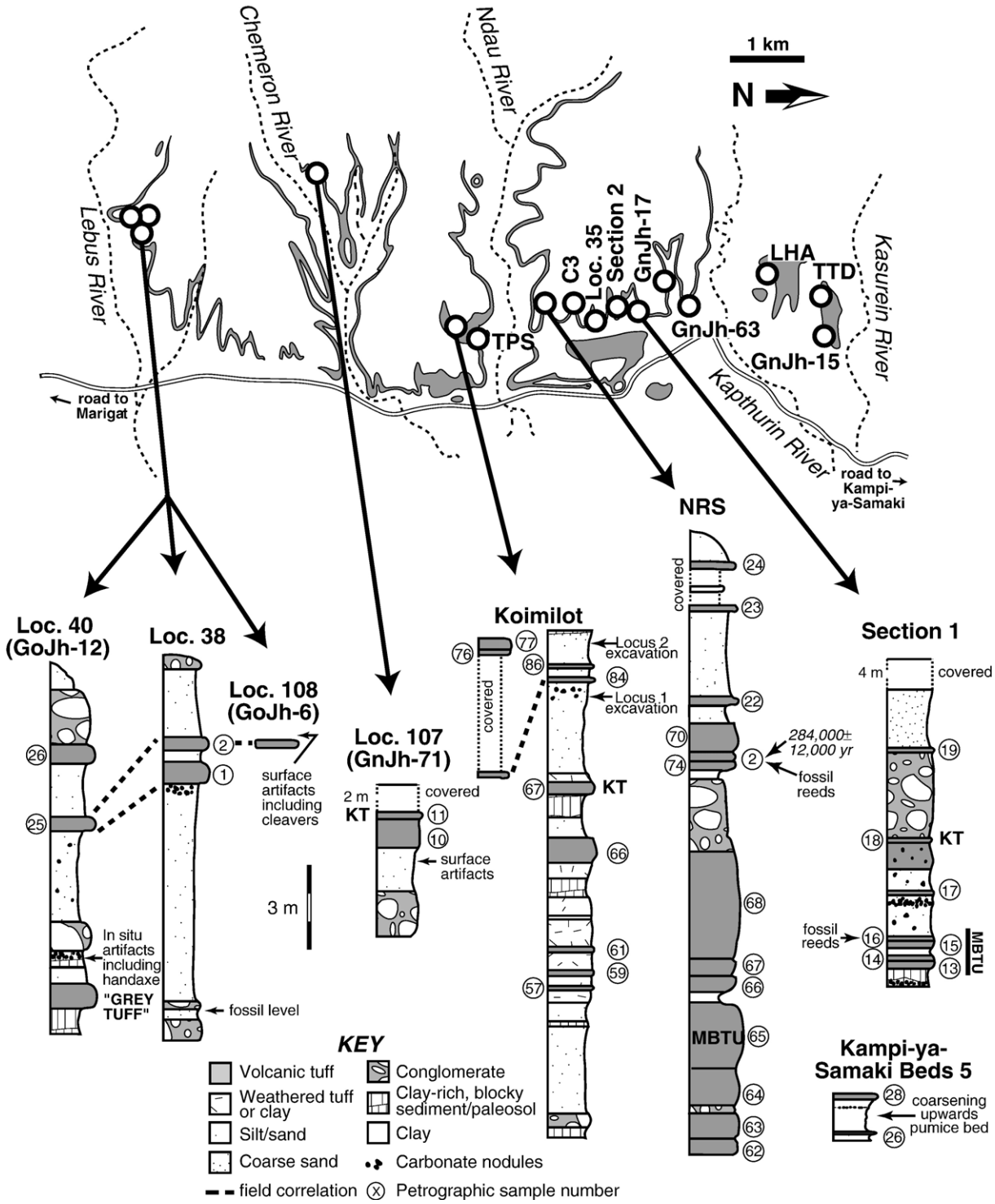

Figure 2. Location of main Bedded Tuff Member (K4) exposures with sampling localities shown. K4 outcrop shown in grey; base map after Tallon (1976). Also shown are schematic stratigraphic sections of areas sampled in 2001–2002. The MBTU (Massive Buff Tuff Unit) and KT (Koimilot Tuff) are local field marker beds. Section 2, C3, Loc. 35, and TPS grab-sampled only. The location of Kampi-ya-Samaki Beds 5 sampling locale is shown in Figure 1. Remaining sites are described in Tryon and McBrearty (2002). For each sampling locale, abbreviated sample numbers are listed; see Table 2 for details.

variability causing spatial differences in tool discard patterns characteristic among mobile foraging populations in seasonal environments (e.g., Potts et al., 1999).

Ten non-archaeological locales were sampled to increase the number of studied Bedded Tuff Member deposits and to strengthen proposed correlations. They include layers dated by the $^{40}Ar/^{39}Ar$ method and others examined to detail lateral variation within a single bed, to verify the presence of a marker tuff, or to limit long-distance correlation between areas by providing an intervening reference point. Most samples

Table 1
Summary attributes of all tephra sampling localities discussed in text

Name*	Abbreviation or SASES Code	Archaeological attribution or age	Artifacts/Depositional and stratigraphic context	References
Kapthurin Formation archaeological sampling localities				
Koimilot*	GnJh-74	MSA	Two excavated strata (64 m^2) from distal alluvial fan sediments within K4. Artifacts (n = 4376) include preferential and recurrent Levallois cores (n = 7) and flakes (n = 10), and 1 pointed uniface on a cobble.	(Tryon, 2002, 2003, in press(a,b))
Rorop Lingop	GnJi-28	Acheulian (Fauresmith?)/MSA	Systematically collected surface artifact sample (n ~ 850), including <15 each of handaxes, points, and Levallois cores from ~0.2 km^2 lacustrine/near-shore sediments within and immediately overlying K4 tephra.	(McBrearty, 1999; McBrearty et al., 1996; Tryon and McBrearty, 2002)
–	GnJh-15	Acheulian/MSA	Artifacts (n ~ 6500) from >500-m^2 excavation include ~120 single/multiplatform cores, 2 picks, and ~40 shaped tools and tool fragments, ~15 of which are small bifaces, some made on cobbles, from a well-developed paleosol beneath local base of K4.	(McBrearty, 1999; Tryon and McBrearty, 2002)
–	GnJh-63	Acheulian/MSA	Artifacts (n = 88) from a 24-m^2 excavation. Tools include 1 handaxe from immature paleosol within K4, and possible point from within overlying tuff.	(Tryon and McBrearty, 2002)
–	GnJh-17	Acheulian/Sangoan?/MSA	Artifacts (n = 9712) from eight excavated strata (144-m^2). Shaped tools (n = 28) include 3 handaxes, 2 points, and 3 pick/core-axes from paleosols and alluvial sediments beneath local base of K4. One large Levallois flake recovered in situ.	(Cornelissen, 1992)
Leakey Handaxe Area	LHA, GnJh-03	Acheulian	Artifacts (n ~ 1500) from surface (0.3 km^2 area) and 70 m^2 excavation in fluviolacustrine sediments ~3 below local base of K4. Shaped tools (n > 50) include 15 handaxes and 6 cleavers. Assemblage also contains ~75 blades and 15–20 blade cores, 4 large Levallois cores and 18 large Levallois flakes.	(Cornelissen, 1992; Leakey et al., 1969; McBrearty, 1999; Tryon et al., in press)
Locality 107*	Loc. 107, GnJh-71	Acheulian	Surface artifacts (n = 6) include 1 cleaver and 1 Levallois core from alluvial sediments beneath local base of K4.	(Tryon, 2002, 2003)
Locality 108*	Loc. 108, GoJh-6	Acheulian	Surface artifacts (n = 10) include 4 cleavers from alluvial sediments overlying K4 tephra.	(Tryon, 2002, 2003)
Locality 40*	Loc. 40, GoJh-12	Acheulian	In situ and surface artifacts (n = 3) include 1 handaxe from paleosol beneath local base of K4.	(Tryon, 2002, 2003)
Kapthurin Formation non-archaeological sampling localities				
Kampi-ya-Samaki Beds 5*	KyS-5	–	Lacustrine or near-shore sediments.	(Tryon, 2003)
Johnny Leakey's Compound	JLC	$^{40}Ar/^{39}Ar$ date of 235,000 ± 2000 yr	Undetermined depositional context.	(Tryon and McBrearty, 2002)
Test Trench D	TTD	–	Upland area with little sediment accumulation.	(Tryon and McBrearty, 2002)
Section 1*	–	–	Alluvial sediments.	(Tryon, 2003)
Section 2*	–	–	Alluvial sediments.	(Tryon, 2003)
Conglomerate 3*	C3	–	Alluvial sediments.	(Tryon, 2003)
Locality 35*	Loc. 35	–	Undetermined depositional context.	(Tryon, 2003)
Ndau River Section	NRS	$^{40}Ar/^{39}Ar$ date of 284,000 ± 12,000 yr	Alluvial sediments.	(Tryon and McBrearty, 2002)
Tallon's Plant Site*	TPS	–	Undetermined depositional context.	(Tryon, 2003)
Locality 38*	Loc. 38	–	Alluvial sediments.	(Tryon, 2003)

Archaeological sites are either named or appended a SASES code after Nelson (1993). Preliminary estimates of archaeological assemblage sizes are given for sites currently under study (GnJh-15 and Rorop Lingop), or in the case of LHA, where published totals differ from those presently found in the National Museums of Kenya.
*Indicates sites analyzed here for the first time.

from the Kapthurin Formation described here are drawn from a ~16-km^2 area of exposures near the Kampi-ya-Samaki/Marigat road (Fig. 2), with the exception of sampling locales JLC and KyS-5, and the archaeological site of Rorop Lingop, which occur in outcrops to the north (Fig. 1).

Our analyses focused on reference sections at Koimilot and Section 1 (Fig. 2), where extensive portions of the Bedded Tuff Member tephrosequence are preserved, complementing prior study of reference sections at GnJh-15 and NRS reported by Tryon and McBrearty (2002). Fine-grained sediments and some incipient paleosols suggest a predominantly alluvial depositional environment at the 14-m-thick Section 1, where eight tephra layers are exposed (Fig. 2). Grain-size and sediment texture at Koimilot is consistent with an alluvial fan

depositional environment near a fluctuating lake shoreline, where nine tuffs are found in exposures >20 m thick (Fig. 2).

Classification of Bedded Tuff Member deposits

Bedded Tuff Member (K4) tephra consist of two distinct lithologies. Widespread beds of coarse mafic ash are overlain in places by sparse deposits of felsic tephra of variable grain size that are locally pumiceous (Tallon, 1976, 1978). The coarse mafic ash is a vitric–lithic tuff of alkali olivine basaltic composition. Thin-section inspection reveals pale brown glass shards (~0.3 mm), crystals of forsteritic (Mg-rich) olivine (~Fo_{69-84}), plagioclase, rare spinel and magnetite, and microcrystalline basalt and trachyte clasts in a fine-grained, glassy groundmass (Tryon and McBrearty, 2002). Bedded Tuff Member basaltic tephra lack suitable material for precise radiometric dating (Deino and McBrearty, 2002).

Grain size readily subdivides the overlying Bedded Tuff Member felsic deposits into fine and coarse categories (after Schmid, 1981), with additional classification based on the results of geochemical analyses described below. Vitric fine or dust tuffs consist of translucent, siliceous glass shards ≤10 μm derived from a range of magmas of intermediate composition (Table 2). Pumiceous coarse (1/16–2 mm) and lapilli (2–64 mm) tuffs contain glass shards predominantly of trachytic composition and rounded pumice fragments ≤30 mm, in addition to feldspars and pyroxenes (aegerine and titaniferrous augite) (Tryon and McBrearty, 2002). Pumice fragments from JLC and NRS have been dated by $^{40}Ar/^{39}Ar$ by Deino and McBrearty (2002) to 235,000 ± 2000 yr and 284,000 ± 12,000 yr, respectively (Figs. 1B and C).

Methods of geochemical analysis

Multiple grain-specific analyses of Bedded Tuff Member samples using wavelength-dispersive electron microprobe (EMP) analysis allows assessment of sample homogeneity and major-element abundance (Froggatt, 1992; Reed, 1996). EMP analyses of 27 samples from 11 geological and archaeological sites are included in this study (Table 2). From each bed, one or more resin-impregnated polished thin sections were prepared. Approximately five shards per bed were analyzed directly from thin section as a preliminary assessment of glass homogeneity. Samples were subdivided where two distinct glass populations were present. The total available dataset consists of 272 analyses (Tryon, 2003).

Quantitative chemical analyses were acquired using a JEOL-8600A EMP housed at the Kline Geology Laboratory, Yale University. Secondary electron and back-scattered electron imaging capabilities facilitated the detection of compositional heterogeneity within a glass shard, as well as the selection of unaltered glass surfaces for analysis (Reed, 1996). For most major element concentrations under standard analytical conditions, instrumental precision and accuracy are estimated at ~1%. Analyses of the basaltic glass used 15 kV accelerating voltage, 20 nA current, and a 10 μm beam. Samples of trachytic coarse and lapilli tuff were analyzed at 15 kV, 7.5 nA, with a 15 μm beam size to minimize Na and K loss, following the recommendations of Froggatt (1992). Selected samples of each type of tuff were extensively tested for specimen damage resulting from beam intensity, and operating conditions were adjusted accordingly. The small grain size of some of the felsic dust tuffs necessitated a lower current and smaller beam size. These samples were run using 15 kV accelerating voltage and 2.5 nA current with a 10 μm beam. Olivine phenocryst analyses employed the same operating conditions as basaltic glass, with a grain-dependent beam size of 5–10 μm. All analyses employed 10-s count times using off-peak backgrounds with TAP, PET, and LIF crystals. Raw data were converted to concentrations using standard calculations with a PhiRhoZ matrix correction. Standards used for calibration include well-characterized silicate and oxide minerals. Analytical totals less than 100% are not normalized, following the argument of Brown et al. (1992) that this procedure makes unwarranted assumptions about the composition of the parent magma. The difference is due largely to water, easily taken up due to the lack of crystalline structure within glass (e.g., Fisher and Schmincke, 1984; Cerling et al., 1985).

Tephrostratigraphic results

As stressed by Feibel (1999), no single value characterizes glass fragments from a volcanic eruption, which are defined instead by a range of values of various elements. This range may result from instrumental error, post-depositional weathering, or natural variation within the parent magma. Accurate correlation requires a large database and multiple sources of evidence to identify potentially equivalent stratigraphic units. Successive field seasons of data collection and analyses have caused our understanding of the Bedded Tuff Member to be constantly revised. Each phase of fieldwork from 1997 through 2002 has resulted in the discovery of new portions of the tephrosequence, and thus a broad correlative framework is adopted here.

On the basis of stratigraphic, petrographic, and geochemical data, as well as the lateral tracing of beds in the field, samples are assigned to one of eight subdivisions of the Bedded Tuff Member. The subdivisions are (1) lower basaltic tuffs, (2) upper basaltic tuffs, (3) the basaltic 'Massive Buff Tuff Unit' (MBTU), (4) evolved basaltic tuffs, (5) pumiceous trachytic tuffs, (6) felsic dust tuffs, (7) the Koimilot Tuff, and (8) redeposited (?) basaltic tuffs. Each of these subdivisions reflects groups of similar tephra, except for the MBTU and Koimilot Tuff, which are field marker beds. Figure 3 shows attribution of all Kapthurin Formation samples to these eight recognized subdivisions (defined below) in summary stratigraphic sections. The location of each of these sites is shown in Figures 1 and 2.

Bedded Tuff Member basaltic tephra deposits

Because of substantial within-sample variation, individual beds of Bedded Tuff Member basaltic tephra cannot be reliably

Table 2
Summary of electron microprobe analyses

Sample	*n*	SiO_2	TiO_2	Al_2O_3	FeO*	MnO	MgO	CaO	Na_2O	K_2O	P_2O_5	SO_3	Cl	SUM
Basaltic glass														
Koimilot														
CAT01–86	(5)	48.44 ± 0.57	2.72 ± 0.57	14.84 ± 0.78	11.16 ± 0.94	0.20 ± 0.05	4.85 ± 0.75	9.39 ± 0.86	3.69 ± 0.09	1.39 ± 0.30	0.55 ± 0.11	0.10 ± 0.05	NA	97.38 ± 0.54
CAT01–84	(7)	49.71 ± 0.34	3.42 ± 0.36	14.65 ± 0.17	11.47 ± 0.22	0.20 ± 0.02	3.73 ± 0.25	7.78 ± 0.40	3.83 ± 0.20	1.88 ± 0.18	0.68 ± 0.05	0.09 ± 0.03	NA	97.45 ± 0.40
CAT01–76	(6)	48.43 ± 0.52	2.89 ± 0.50	14.28 ± 0.52	11.48 ± 0.84	0.19 ± 0.05	4.82 ± 0.52	9.61 ± 0.85	3.78 ± 0.32	1.40 ± 0.22	0.57 ± 0.06	0.08 ± 0.04	NA	97.57 ± 0.18
CAT01–77	(6)	48.82 ± 0.32	2.20 ± 0.10	15.46 ± 0.25	9.92 ± 0.24	0.15 ± 0.04	5.84 ± 0.23	10.51 ± 0.25	3.51 ± 0.11	1.31 ± 0.09	0.47 ± 0.03	0.06 ± 0.04	NA	98.33 ± 0.47
CAT01–66	(4)	48.52 ± 0.30	2.69 ± 0.12	14.46 ± 0.32	11.14 ± 0.20	0.18 ± 0.05	4.65 ± 0.08	9.54 ± 0.07	3.55 ± 0.23	1.56 ± 0.04	0.56 ± 0.02	0.10 ± 0.03	NA	96.97 ± 0.65
CAT01–59	(6)	48.99 ± 0.36	2.23 ± 0.06	15.20 ± 0.32	10.45 ± 0.42	0.19 ± 0.03	5.36 ± 0.11	9.73 ± 0.11	3.71 ± 0.17	1.18 ± 0.04	0.44 ± 0.04	0.07 ± 0.04	NA	97.56 ± 0.77
CAT01–57	(6)	49.38 ± 0.26	2.45 ± 0.17	15.14 ± 0.40	10.73 ± 0.28	0.18 ± 0.04	5.03 ± 0.36	9.35 ± 0.08	3.69 ± 0.15	1.30 ± 0.06	0.52 ± 0.06	0.07 ± 0.03	NA	97.85 ± 0.38
Section 1														
CAT02–19	(4)	50.90 ± 1.09	3.25 ± 0.33	15.13 ± 0.41	10.99 ± 0.77	0.22 ± 0.05	3.56 ± 0.20	7.03 ± 0.48	3.91 ± 0.18	2.13 ± 0.14	0.70 ± 0.05	0.09 ± 0.01	NA	97.89 ± 0.29
CAT02–17	(6)	48.91 ± 0.12	2.29 ± 0.07	15.57 ± 0.19	10.78 ± 0.16	0.20 ± 0.03	5.45 ± 0.09	9.51 ± 0.08	3.80 ± 0.06	1.19 ± 0.02	0.49 ± 0.04	0.07 ± 0.02	NA	98.25 ± 0.27
CAT02–16	(6)	49.33 ± 0.44	2.27 ± 0.12	15.28 ± 0.32	10.55 ± 0.20	0.18 ± 0.05	5.28 ± 0.09	9.72 ± 0.09	3.74 ± 0.09	1.20 ± 0.03	0.44 ± 0.04	0.08 ± 0.03	NA	98.08 ± 0.60
CAT02–15	(6)	48.48 ± 0.43	2.11 ± 0.16	15.70 ± 0.37	10.22 ± 0.20	0.19 ± 0.03	5.94 ± 0.39	10.11 ± 0.29	3.81 ± 0.06	1.00 ± 0.15	0.42 ± 0.07	0.07 ± 0.02	NA	98.06 ± 0.54
CAT02–14a	(3)	49.04 ± 0.18	2.13 ± 0.05	15.79 ± 0.26	9.94 ± 0.23	0.18 ± 0.06	5.90 ± 0.19	9.46 ± 0.38	3.83 ± 0.18	1.18 ± 0.07	0.45 ± 0.01	0.08 ± 0.03	NA	98.03 ± 0.14
CAT02–14b	(3)	49.36 ± 0.26	2.55 ± 0.02	14.9 ± 0.20	10.74 ± 0.32	0.21 ± 0.05	4.99 ± 0.07	9.31 ± 0.07	3.61 ± 0.12	1.35 ± 0.02	0.54 ± 0.01	0.07 ± 0.02	NA	97.71 ± 0.29
CAT02–13	(6)	48.64 ± 0.33	2.26 ± 0.03	15.41 ± 0.07	10.23 ± 0.14	0.21 ± 0.04	5.40 ± 0.09	9.61 ± 0.11	3.90 ± 0.09	1.22 ± 0.03	0.54 ± 0.05	0.08 ± 0.02	NA	97.53 ± 0.51
Loc. 38														
CAT02–02	(6)	49.00 ± 0.45	2.58 ± 0.09	14.76 ± 0.19	10.89 ± 0.49	0.20 ± 0.02	4.73 ± 0.18	9.53 ± 0.22	3.63 ± 0.12	1.53 ± 0.06	0.56 ± 0.03	0.09 ± 0.05	NA	97.53 ± 0.54
CAT02–01	(6)	48.96 ± 0.40	2.37 ± 0.04	15.34 ± 0.17	10.98 ± 0.25	0.21 ± 0.03	5.25 ± 0.24	9.38 ± 0.15	3.67 ± 0.14	1.26 ± 0.04	0.47 ± 0.03	0.09 ± 0.03	NA	98.00 ± 0.63
Kampi-ya-Samaki Beds Section 5														
CAT02–28	(5)	51.12 ± 0.18	2.88 ± 0.14	14.78 ± 0.38	11.55 ± 0.25	0.25 ± 0.04	3.34 ± 0.11	7.02 ± 0.05	3.78 ± 0.13	1.95 ± 0.93	1.16 ± 0.05	0.12 ± 0.02	NA	97.96 ± 0.40
CAT02–26a	(3)	47.86 ± 0.29	2.96 ± 0.37	14.60 ± 0.48	12.36 ± 0.44	0.21 ± 0.02	4.62 ± 0.54	9.27 ± 0.52	3.68 ± 0.16	1.38 ± 0.14	0.57 ± 0.08	0.13 ± 0.05	NA	97.67 ± 0.50
CAT02–26b	(5)	52.52 ± 0.66	2.53 ± 0.15	14.68 ± 0.61	10.37 ± 0.11	0.23 ± 0.05	2.83 ± 0.24	5.99 ± 0.35	4.28 ± 0.26	2.52 ± 0.24	1.04 ± 0.05	0.08 ± 0.04	NA	97.09 ± 0.86
Siliceous glass														
NRS														
CAT02–23	(6)	58.08 ± 0.60	0.21 ± 0.13	15.98 ± 0.11	6.24 ± 0.42	ND	ND	1.48 ± 0.10	6.00 ± 1.20	4.87 ± 0.23	ND	NA	0.19 ± 0.07	93.75 ± 2.16
CAT02–22	(6)	57.38 ± 1.11	0.25 ± 0.06	15.77 ± 0.43	6.08 ± 0.48	0.26 ± 0.08	ND	1.73 ± 0.18	6.53 ± 0.53	5.04 ± 0.28	ND	NA	0.17 ± 0.06	93.65 ± 1.34
Loc. 35														
CAT02–21	(6)	59.31 ± 0.53	0.45 ± 0.09	13.84 ± 0.39	7.14 ± 0.27	0.21 ± 0.13	ND	1.19 ± 0.14	7.45 ± 1.01	4.61 ± 0.22	ND	NA	0.15 ± 0.06	95.06 ± 1.81
TPS														
CAT01–55	(5)	58.31 ± 0.58	0.17 ± 0.10	15.63 ± 0.16	6.77 ± 0.79	0.25 ± 0.05	ND	1.05 ± 0.29	8.54 ± 0.78	4.77 ± 0.35	ND	NA	0.33 ± 0.08	96.59 ± 1.29
C3														
CAT02–25	(6)	60.04 ± 0.53	0.50 ± 0.10	14.10 ± 0.40	7.53 ± 0.45	0.26 ± 0.22	ND	1.03 ± 0.20	7.38 ± 1.25	4.44 ± 0.18	ND	NA	0.16 ± 0.03	96.02 ± 1.75
Koimilot														
CAT01–67	(10)	59.79 ± 0.64	0.59 ± 0.07	11.46 ± 0.19	8.80 ± 0.54	0.39 ± 0.16	0.10 ± 0.04	0.81 ± 0.07	4.13 ± 2.76	3.89 ± 0.45	ND	NA	0.38 ± 0.07	91.05 ± 3.52
Section 1														
CAT02–18	(14)	59.66 ± 0.82	0.53 ± 0.10	11.41 ± 0.40	8.94 ± 0.60	0.35 ± 0.09	0.10 ± 0.04	0.80 ± 0.08	5.83 ± 2.27	3.89 ± 0.74	ND	NA	0.38 ± 0.07	92.57 ± 3.25
Section 2														
CAT02–20	(5)	59.74 ± 0.26	0.62 ± 0.06	11.61 ± 0.21	9.15 ± 0.31	0.45 ± 0.13	0.11 ± 0.02	0.79 ± 0.05	7.89 ± 1.43	4.21 ± 0.22	ND	NA	0.41 ± 0.04	95.77 ± 2.12
Loc. 107														
CAT01–11	(6)	60.13 ± 0.62	0.53 ± 0.10	11.55 ± 0.36	8.43 ± 0.47	0.29 ± 0.14	0.10 ± 0.06	0.77 ± 0.09	2.85 ± 1.17	3.11 ± 0.83	ND	NA	0.38 ± 0.03	88.91 ± 2.13
Loc. 40														
CAT01–26	(3)	60.98 ± 0.87	0.59 ± 0.25	11.51 ± 1.31	7.85 ± 0.97	0.38 ± 0.25	ND	0.72 ± 0.05	6.41 ± 2.10	4.24 ± 0.18	ND	NA	0.37 ± 0.07	93.48 ± 2.67

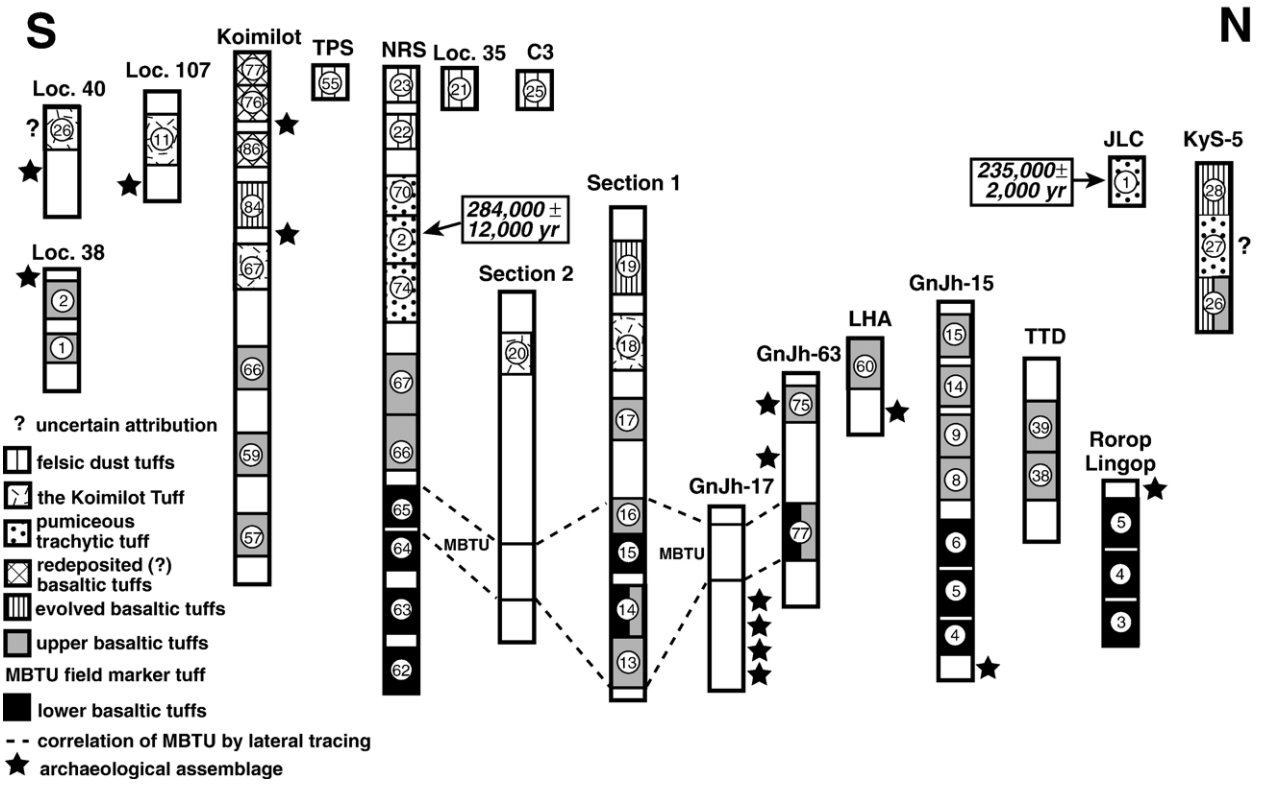

Figure 3. Schematic stratigraphic sections showing analyzed tephra samples and classification of Bedded Tuff Member units. Stars denote position of archaeological assemblage(s) at each locale. Circled numbers are abbreviated sample numbers listed in Table 2 and from Tryon and McBrearty (2002). Note that the MBTU field marker tuff is present at both Section 2 and GnJh-17, where it is laterally correlated in the field with chemically analyzed samples from NRS, Section 1, and GnJh-63. Sections not to scale; aligned roughly along a north–south axis. White areas include non-volcaniclastic sediments not used for correlation. See Figures 1 and 2 for site locations.

correlated among exposures on the basis of geochemical composition alone. Mean elemental oxide abundance between stratigraphically adjacent units frequently overlaps at one standard deviation (see Table 2 and Tryon and McBrearty, 2002). Instead, samples are assigned to one of three geochemical variants of basaltic glass, with each variant defined primarily on the basis of MgO abundance (Fig. 4). Two of these variants were termed by Tryon and McBrearty (2002) 'lower' and 'upper' basaltic tuffs on the basis of their stratigraphic position at reference sections GnJh-15 and NRS (Fig. 3). Lower and upper basaltic tuffs are defined by a compositional gap between ~5.5 and 6 wt.% MgO (Fig. 4). Upper basaltic tuffs have increased average values of wt.% FeO and TiO_2 and smaller amounts of wt.% CaO. These differences are not accompanied by a major change in SiO_2, which remains ~48–49 wt.%. Compositional change within the upper and lower basaltic tuff geochemical variants follows a similar trend (Fig. 4). Olivine phenocrysts from lower and upper basaltic tuffs range from ~$Fo_{78–84}$ (Table 3).

The third basaltic tuff geochemical variant, recognized here for the first time, is demarcated by a compositional gap between ~3.7 and 4.2 wt.% MgO (Fig. 4). Weight percent TiO_2 and FeO differ little from the upper basaltic tuffs, but an inflection in the trend of these element oxides probably reflects the initial crystallization of magnetite (Fig. 4). Average wt.% CaO values are lower than samples assigned to both the upper and lower basaltic variants. Weight percent SiO_2 is ~49–50%, and olivine composition is ~$Fo_{69–74}$ (Tables 2 and 3). Higher wt.% SiO_2, reduced amounts of CaO, and more iron-rich olivine phenocrysts indicate a less primitive magma for these samples relative to that which produced the upper and lower basaltic tuffs (see McBirney, 1984). Samples attributed to this variant are thus termed 'evolved' basaltic tuffs. Evolved basaltic tuffs do not occur at GnJh-15 or NRS but overlie upper basaltic tuffs at Koimilot and Section 1 (Fig. 3).

The lower, upper, and evolved basaltic tuffs that compose a portion of the Bedded Tuff Member together form a useful correlation tool within the Kapthurin Formation. Bivariate plots of oxide values show discrete patterning (Fig. 4), and there is a consistent stratigraphic relationship among the three basaltic tuff variants at reference sections GnJh-15, NRS, Section 1, and

Notes to Table 2:
Samples from each locale listed in stratigraphic order. Results, including analytical totals, are listed as mean and one standard deviation. All analyses as wt.%. *n* = number of glass shards analyzed per sample. (a) and (b) denote subsets of a single sample with multiple chemically discrete glass populations. NA = not analyzed, ND = not detected. Also analyzed but below detection limits were Cr, Ni, Ba, and F. *Total Fe as FeO.

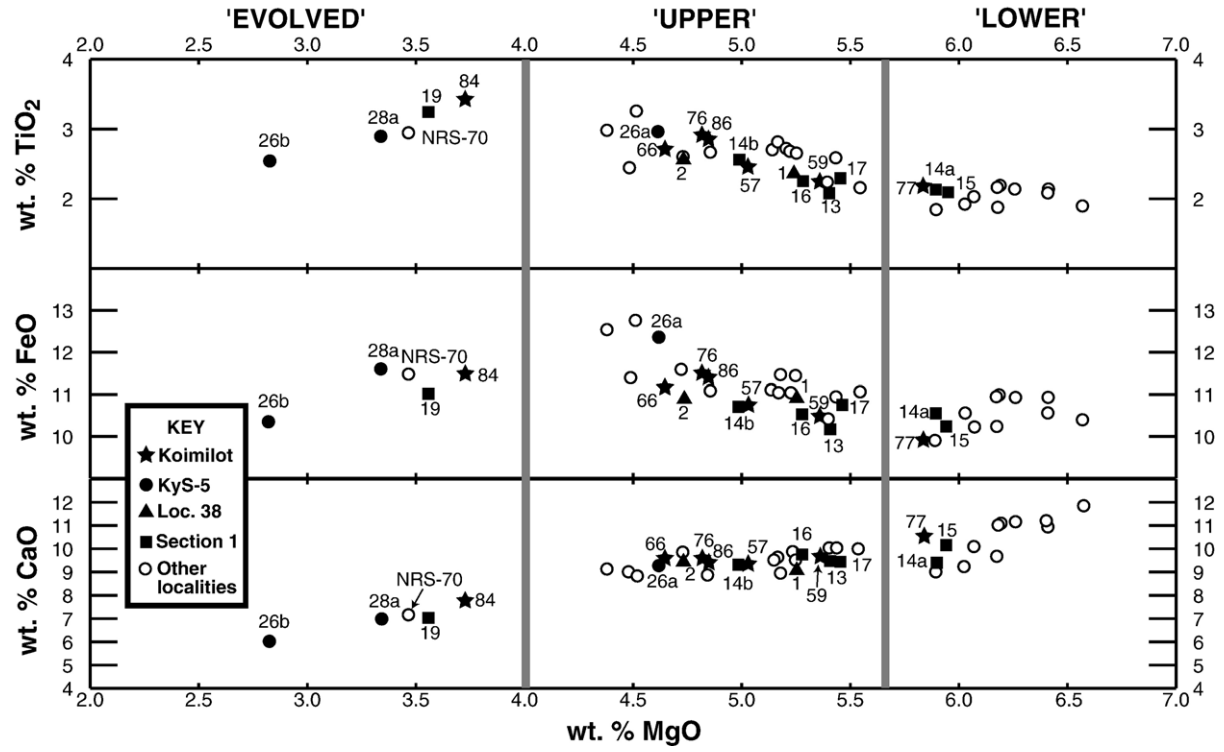

Figure 4. Oxide variation diagram for all sample means of Bedded Tuff Member (K4) basaltic tephra deposits. Sample numbers are abbreviated; see Table 2 for details. Compositional basis for distinguishing 'evolved,' 'upper,' and 'lower' basaltic portions of K4 shown. Results of K4 tephra analyses from Tryon and McBrearty (2002) are shown as open circles for comparison. Only sample CAT97–70 from NRS has changed attribution; originally identified as an upper basaltic tuff, this sample is now attributed to the evolved basaltic tuff subdivision.

Koimilot (Fig. 3), with lower basaltic tuffs at the base overlain in turn by upper and evolved basaltic tuffs. Successive field seasons have shown that the 'gaps' that define each of the basaltic variants result in part from sampling bias due to stratigraphic incompleteness and suggest that these are arbitrary divisions within a continuum.

Lateral tracing of the highly distinctive 'Massive Buff Tuff Unit' (MBTU) field marker bed provides an additional means of correlation among exposures (Fig. 3). However, recent detailed study demonstrates that the MBTU is not an isochronous horizon. The MBTU has a thickness of ~3 m and consists of multiple beds of varying basaltic composition, in places intercalated with terrigenous sediment, as at Section 1 (Figs. 2 and 3). Evidence for stratification of these beds is now often absent due to post-depositional homogenization by turbation and possibly redeposition, as at Section 2 (Fig. 2), resulting in beds such as CAT02–14 with 'mixed' samples with glass shards of both lower and upper basaltic compositions overlain by lower basaltic tephra (Table 2). The MBTU probably records a prolonged period between eruptions dominated by pedogenesis and alluvial rather than volcaniclastic sedimentation (e.g., Smith, 1991). The MBTU illustrates the more general problem affecting Bedded Tuff Member deposits that renders correlation of individual beds difficult. Airfall tephra settled into an active alluvial environment, resulting in minor reworking of volcaniclastic sediment and epiclastic admixture. Therefore, discrete tephra layers observable in the field rarely correspond to individual eruptive events.

Bedded Tuff Member (K4) felsic tephra

The Koimilot Tuff field marker bed is the most widespread of the felsic tuffs within the Bedded Tuff Member, and unlike most K4 tephra, the Koimilot Tuff likely records a single eruptive and depositional event preserved at multiple outcrops. Samples were attributed to the Koimilot Tuff in the field on the basis of stratigraphic position, coarse silt texture, and characteristic olive-grey color (Munsell 5Y 6.5/2 dry and 5Y 4.5/3 wet). Microprobe analyses (n = 35) of Koimilot Tuff samples from Koimilot (CAT01–67), Loc. 107 (CAT01–11), Section 1 (CAT02–18), and Section 2 (CAT02–20) are compositionally distinct and exhibit little inter- or intra-sample variability (Fig. 5 and Table 2). Samples are fine-grained (~10 μm) vitric tuffs, with rare aegerine and feldspar grains and sparse trachyte lithic fragments. Sample CAT01–16 from Loc. 40 (Fig. 3) is a vitric tuff composed of highly vesicular rounded glass shards ~40 μm in diameter, with rare aegerine and feldspar phenocrysts. This bed is chemically similar to the Koimilot Tuff, but exhibits slight chemical differences from other samples assigned to the Koimilot Tuff, and may represent a coarser facies.

The Koimilot Tuff is exceptional, as glass major and minor element geochemical composition provides little basis for correlating other non-basaltic, siliceous tephra within the Bedded Tuff Member. As seen in Figure 5, no elemental oxide combinations consistently discriminate between the felsic dust tuffs and the pumiceous trachytic tuffs described by Tryon

Table 3
Results of electron microprobe analyses of olivine phenocrysts in tephra of the Bedded Tuff Member

Location	Sample	K4 geochemical variant	Fo
Koimilot	CAT01–84	Evolved basaltic tuffs	73.9
Koimilot	CAT01–84	Evolved basaltic tuffs	71.2
Koimilot	CAT01–84	Evolved basaltic tuffs	71.3
Koimilot	CAT01–84	Evolved basaltic tuffs	72.5
Section 2	CAT02–19	Evolved basaltic tuffs	70.7
Section 2	CAT02–19	Evolved basaltic tuffs	69
GnJh-15	CAT97–14	Upper basaltic tuffs	80.4
GnJh-15	CAT97–10	Upper basaltic tuffs	78.8
GnJh-15	CAT97–09	Upper basaltic tuffs	80.4
GnJh-15	CAT97–09	Upper basaltic tuffs	84.1
Test Trench D	CAT97–38	Upper basaltic tuffs	78.4
Test Trench D	CAT97–38	Upper basaltic tuffs	79.6
Test Trench D	CAT97–38	Upper basaltic tuffs	80.5
Test Trench D	CAT97–39	Upper basaltic tuffs	80.7
Test Trench D	CAT97–39	Upper basaltic tuffs	80.7
Test Trench D	CAT97–39	Upper basaltic tuffs	80.4
LHA	CAT97–60	Upper basaltic tuffs	82.6
LHA	CAT97–60	Upper basaltic tuffs	81.4
LHA	CAT97–60	Upper basaltic tuffs	75.3
Section 1	CAT02–17	Upper basaltic tuffs	81.5
Koimilot	CAT01–57	Upper basaltic tuffs	77.9
Koimilot	CAT01–57	Upper basaltic tuffs	81
Koimilot	CAT01–57	Upper basaltic tuffs	82.2
Section 1	CAT02–16	Upper basaltic tuffs/MBTU	81.5
Section 1	CAT02–16	Upper basaltic tuffs/MBTU	82.9
Section 1	CAT02–16	Upper basaltic tuffs/MBTU	79.5
NRS	CAT97–64	Lower basaltic tuffs	83.1
Koimilot	CAT01–76	Redeposited (?)/upper basaltic tuffs	80.8
Koimilot	CAT01–76	Redeposited (?)/upper basaltic tuffs	73.9
Koimilot	CAT01–76	Redeposited (?)/upper basaltic tuffs	85.8
Koimilot	CAT01–77	Redeposited (?)/lower basaltic tuffs	82.2
Koimilot	CAT01–77	Redeposited (?)/lower basaltic tuffs	84.6

Analyzed elements include: Si, Ti, Al, Fe, Mn, Mg, Ca, Cr, and Ni. Ordered by basaltic glass subdivision, reported as mole percent forsterite (Fo) and calculated by stoichiometry.

and McBrearty (2002), or provide correlation between exposures.

Explanation of compositional trends: a hypothesis

Tryon and McBrearty (2002) suggest a shared magma source for the lower and upper basaltic tuffs and the pumiceous trachytic tephra deposits of the Bedded Tuff Member on the basis of the similar geochemical trends and the stratigraphic superposition of tephra of increasingly evolved compositions. Proportions of MgO and CaO decrease with stratigraphic height, from lower to upper to pumiceous trachytic tuffs, with concomitant increases in FeO and TiO_2 (Figs. 4 and 6). This model is supported and augmented by results presented here. The stratigraphic position of evolved basaltic tuffs is demonstrated at Koimilot and Section 1, where they overlie upper basaltic tephra (Figs. 2–4). These evolved basaltic tuffs conform to the same chemical trend observed for all lower and upper basaltic as well as pumiceous trachytic deposits of K4 (Fig. 6). The general trend in compositional variation among the basaltic layers is interpreted as the result of chemical evolution of a magma chamber over time. Temporal changes in magma composition are recorded in successive deposits from periodic eruptions. A linear trend of reduced MgO and CaO (Fig. 6) is consistent with fractionation due to crystallization of olivine (Table 3) and plagioclase phenocryst phases, and suggests a progression from lower through upper to evolved basaltic composition. A shared volcanic source for the basaltic and trachytic tephra is further suggested by the presence of evolved basaltic glass shards within pumiceous trachytic tuff samples from NRS (Tryon, 2003: Appendix B). Furthermore, the sample from JLC is a single pumice fragment of trachytic and evolved basaltic glass apparently fused together during magma ascent (Tryon and McBrearty, 2002).

The overall stratigraphic and compositional trend of basalts with increasingly evolved compositions, followed by mixed basalt/trachyte eruptions, parallels observations of volcano evolution and magma differentiation in the East African Rift and elsewhere. Bimodal suites of alkali basalt–trachyte lava characterize all Kenyan Pleistocene central Rift Valley volcanoes north of Lake Baringo, including Korosi (Fig. 1), the inferred source of the Bedded Tuff Member basaltic and pumiceous trachytic deposits. In each case, lavas are separated by a compositional gap of up to 15 wt.% SiO_2, known as the 'Daly gap,' common in alkaline igneous suites (Tallon, 1978; Baker, 1987; Macdonald, 1987; Philpotts, 1990; Dunkley et al., 1993; Orton, 1996). Thus, unlike the gaps between the lower and upper basaltic tuffs, the absence of tuffs of compositions intermediate between the basaltic and trachytic portions of the Bedded Tuff Member (Fig. 6) need not record an erosional unconformity or the absence of preserved strata, but rather reflects the nature of the volcanic process itself.

Two tephra groups do not conform to the observed trends: (1) fine-grained tephra with siliceous glass fragments, including the felsic dust tuffs and the Koimilot Tuff, and (2) the uppermost basaltic tuffs at Koimilot. Felsic dust tuffs overlie pumiceous trachytic tuffs at NRS but are otherwise known only from isolated beds from locales in the vicinity of the Ndau River (Figs. 2 and 3). No section preserves both the Koimilot Tuff and pumiceous trachytic tuffs. The felsic dust tuffs from NRS (CAT02–22 and CAT02–23) are not clearly associated with the inferred sequence of a single differentiating volcanic source (Figs. 5 and 6). These samples do not fall along the compositional trend line (MgO:CaO) that defines other Bedded Tuff Member samples (Fig. 6 inset). These data, plus differences in chemical composition (Fig. 5, Table 2) and smaller average grain size ($\leq$10 μm), suggest a different, more distant volcanic source for the felsic dust tuffs and the Koimilot Tuff than the pumiceous trachytic samples of the Bedded Tuff Member.

Tephra beds above the Koimilot Tuff at the site of Koimilot (Fig. 3) show a reversal of the general stratigraphic and compositional trend. The lowermost of these, CAT01–84, is of evolved basaltic composition. Glass chemical composition of samples CAT01–86 and CAT01–76 match those of upper basaltic tuffs, overlain by CAT01–77, which is similar to other

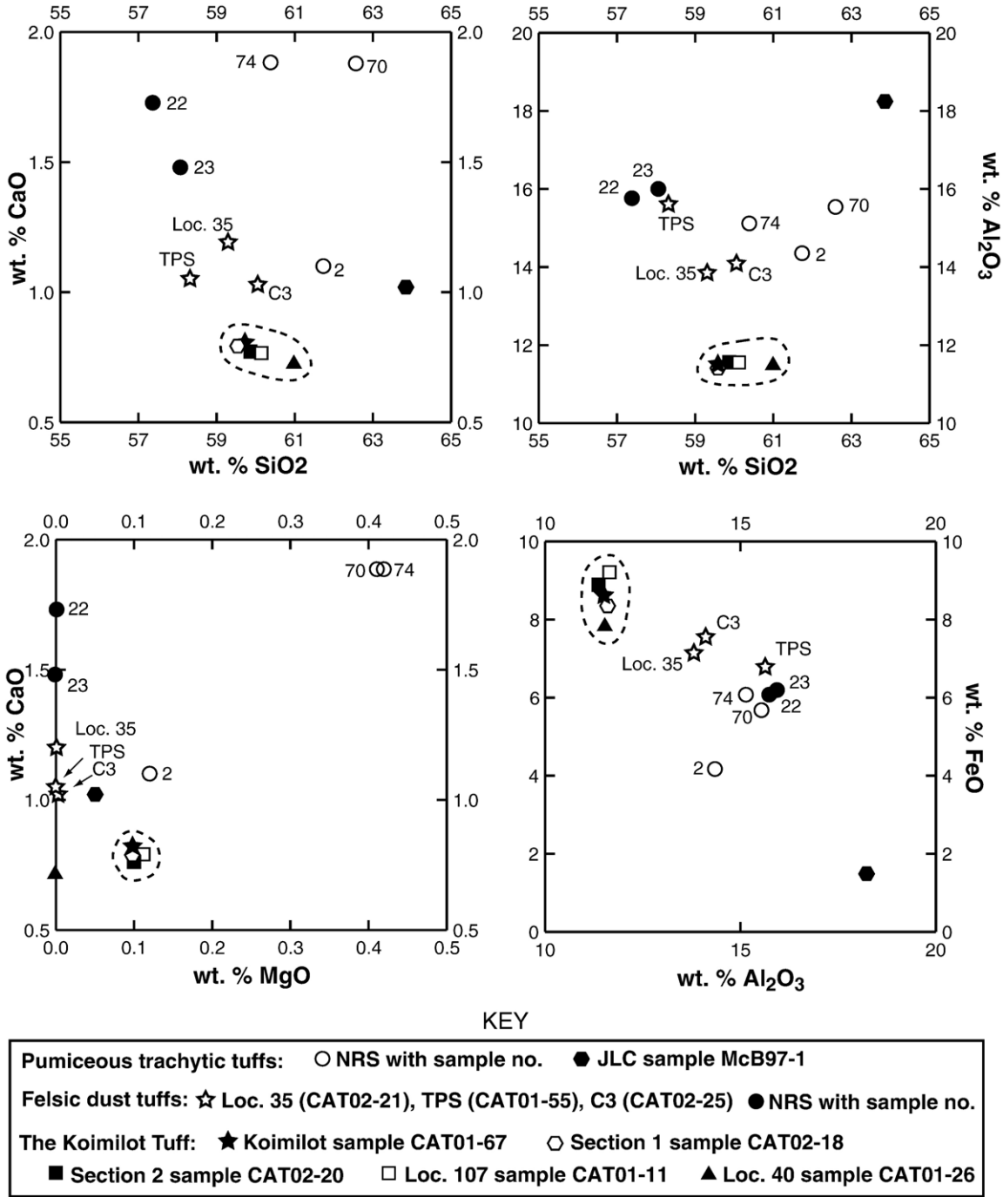

Figure 5. Bivariate plots of sample means of all siliceous (non-basaltic) glass samples from the Bedded Tuff Member. Dashed line encircles samples attributed to the Koimilot Tuff. Glass chemistry of sample CAT01–26 from Loc. 40 is compositionally similar to other samples of the Koimilot Tuff but petrographically distinct. See text for discussion.

lower basaltic tuffs (Figs. 3 and 4). This pattern is not found at any other stratigraphic section. It may result from erosion and redeposition of beds of upper and lower basaltic tuffs, and they are therefore termed redeposited (?) basaltic tuffs. Thin section evidence showing rounded glass shards in all these samples except CAT01–77 provides some support for this interpretation. Alternatively, these tephra may record later, unrelated phases of basaltic volcanism not preserved elsewhere in the Kapthurin Formation.

Age and stratigraphic summary of the Bedded Tuff Member (K4)

Figure 7 presents a summary of known stratigraphic relations of the eight recognized subdivisions of the Bedded Tuff Member (K4) and emphasizes the differential preservation of portions of the complete K4 sequence at different reference locales north and south of the Ndau River, shown here as composite stratigraphic sections based on NRS and Koimilot.

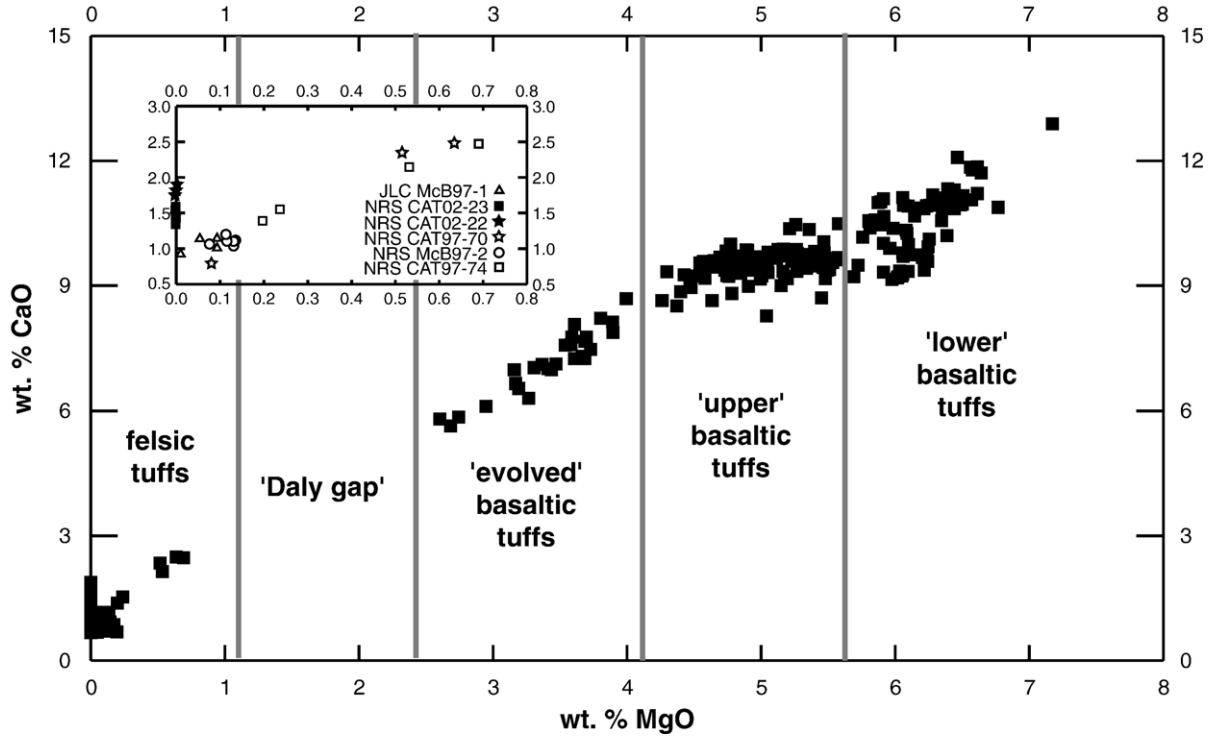

Figure 6. All Bedded Tuff Member analyses of glass (n = 272). Single compositional trend among basaltic and trachytic samples suggest common volcanic origin. Inset shows all analyses of siliceous (non-basaltic) glass from dated sections at JLC and NRS, listed in stratigraphic order for NRS. In the inset, pumiceous trachytic tuffs shown as open symbols, felsic dust tuffs as filled symbols.

Deposits of pumiceous trachytic tuffs at NRS and JLC have $^{40}Ar/^{39}Ar$ age estimates of 284,000 ± 12,000 yr and 235,000 ± 2000 yr, respectively (Deino and McBrearty, 2002). The younger age from JLC is consistent with its more evolved geochemical signature and the inferred common volcanic source of both dated samples. The 284,000 ± 12,000 yr date provides a minimum age for the upper and lower basaltic tuffs, as well as the Massive Buff Tuff Unit (MBTU), all found beneath the dated stratum at NRS (Figs. 3 and 7). The relative stratigraphic sequence of upper basaltic tuffs overlain by the Koimilot Tuff and evolved basaltic tuffs is established at both Section 1 and Koimilot (Figs. 3 and 7). However, neither the Koimilot Tuff nor tephra beds of evolved basaltic composition are present at either of the dated sections, NRS and JLC.

On the basis of the observed geochemical trend (Fig. 6), evolved basaltic tuffs are likely older than the dated trachytic tephra. Evidence of mixed basaltic/trachytic deposits was noted above, and at KyS-5, sample CAT02–26 contains mixed upper and evolved basaltic glass and underlies a coarse pumiceous bed of undetermined composition similar to the dated deposits, which is in turn overlain by additional evolved basaltic tuffs (Figs. 1–3). These observations suggest the presence of alternating phases of basaltic and trachytic eruptions between ~284,000 yr and ~235,000 yr. The Koimilot Tuff, which underlies an evolved basaltic tuff at Koimilot and Section 1, is therefore likely older than or contemporary with one or both of the dated pumiceous deposits. On this basis, the age of the Koimilot Tuff is estimated here at ~250,000 yr, pending confirmation by future direct stratigraphic correlation or isotopic dating. The age of the felsic dust tuffs is unknown, except for the relative position of those that overlie the dated level at NRS. Upper age limits for the Bedded Tuff Member remain poorly constrained, but as noted above, age estimates of 198,000–345,000 yr for the major faulting episode that marks the end of Kapthurin Formation sediment deposition suggests a late middle Pleistocene age for all geological strata and archaeological assemblages discussed here.

Archaeological sites and implications

Figure 7 shows the stratigraphic relations among the eight subdivisions of the Bedded Tuff Member and the archaeological assemblages discussed here. The results of the chronological ordering of sites in the Kapthurin Formation directly contributes to our understanding of the age of the earliest Middle Stone Age (MSA), the technological variation among later middle Pleistocene eastern African archaeological sites, and the nature of the Acheulian–MSA transition. Most archaeological assemblages, particularly those north of the Ndau River, occur within or beneath upper basaltic tuffs. Upper basaltic tuffs underlie dated pumiceous trachytic deposits at NRS and are thus older than 284,000 ± 12,000 yr (Fig. 7). Points are a rare but conspicuous feature of the GnJh-17 excavations from beneath the MBTU (Fig. 7, Table 1). Because points are considered the diagnostic tool type of the MSA, their presence in levels dated >284,000 yr suggests greater antiquity for the beginning of the MSA in the Kapthurin Formation than found elsewhere in Africa (McBrearty and Tryon, 2006).

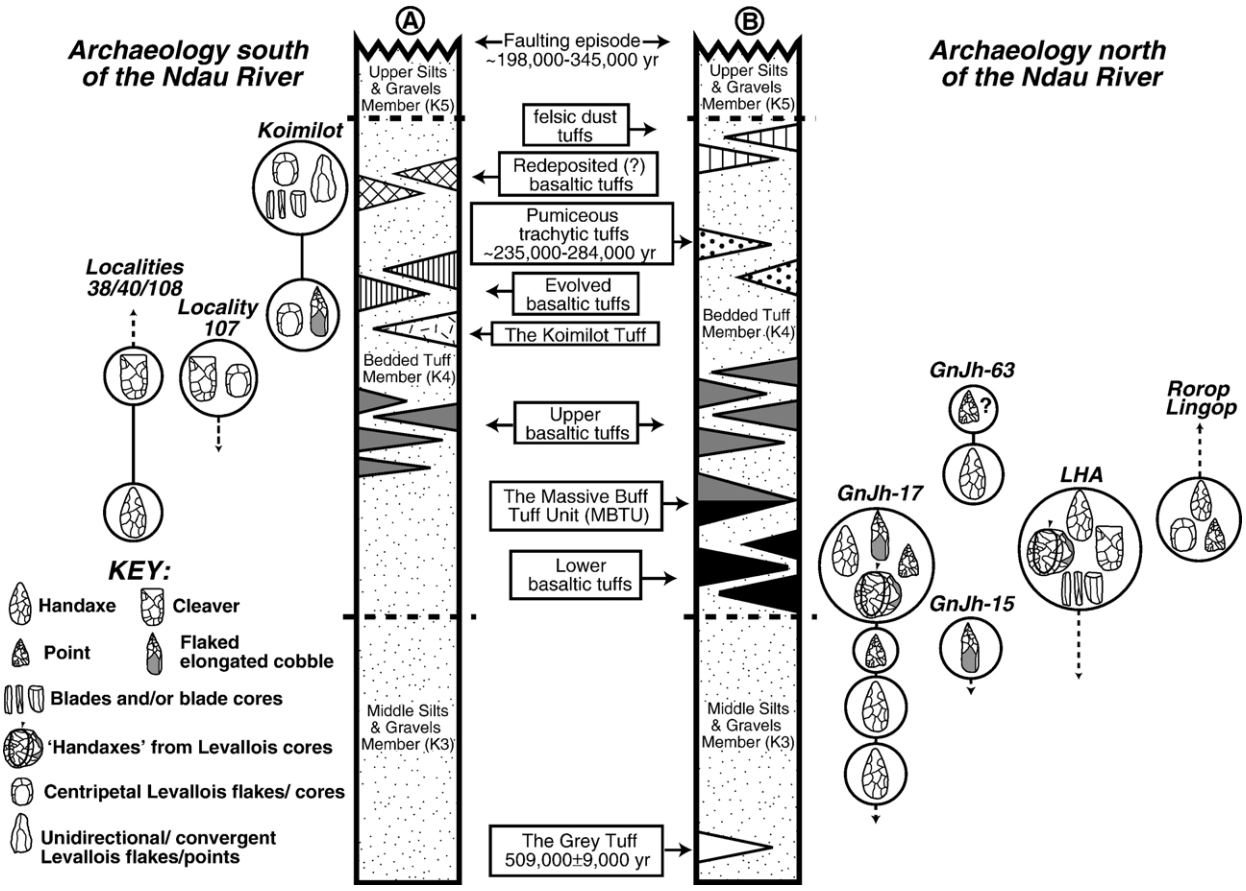

Figure 7. Summary stratigraphic relations of archaeological assemblages and Bedded Tuff Member subdivisions, the latter recognized on the basis of field, petrographic, and geochemical criteria. The number of tuffs shown is schematic, except for the field marker units the MBTU and the Koimilot Tuff. Sections are not to scale. Stratigraphic sections A and B are composites, emphasizing the differential preservation of portions of the Bedded Tuff Member sequence that affects the stratigraphic ordering of archaeological assemblages. Section A is based on the sequence observed at Koimilot, Section B based on the NRS succession. Note that the stratigraphic relation of the Koimilot Tuff and evolved basaltic tuffs to the dated pumiceous trachytic tuffs and the felsic dust tuffs is uncertain. Stippled pattern denotes the variable presence of intervening non-volcaniclastic sediments, which are absent at some locales such as GnJh-15. Dashed arrows denote range of stratigraphic positions due to absence of overlying or underlying tephra. Artifact icons after Tryon and McBrearty (2002).

In the Kapthurin Formation, it is clear that the two elements characteristic of the MSA, points and Levallois flake production, do not co-occur at all MSA assemblages, nor do they appear synchronously in the archaeological record. Despite their early age, points are interstratified with typical Acheulian tools such as handaxes in strata beneath upper basaltic tuffs. Interstratification of points and handaxes is visible at sites GnJh-17 and GnJh-63, linked by lateral field tracing of the Massive Buff Tuff Unit (MBTU) (Fig. 3). Points and handaxes also co-occur in the same archaeological level at GnJh-17 and Rorop Lingop (Fig. 7). Recent finds at Loc. 108 show the presence of cleavers in strata overlying upper basaltic tuffs, and in combination these observations show the persistence of Acheulian tool manufacture well after the introduction of points (Fig. 7). Although Levallois flake production is considered one of the hallmarks of the MSA, the earliest examples of Levallois technology in the Kapthurin Formation occurs at an Acheulian site, the Leakey Handaxe Area (LHA), found ~3 m beneath an upper basaltic tuff (Fig. 7). At LHA, lava boulders were shaped by centripetal flaking for the production of a single large (~10–20 cm) Levallois flake. These were then transformed by retouch into handaxes, cleavers, or similar implements (Leakey et al., 1969; Tryon, in press(b), Tryon et al., in press). As described below, MSA Levallois technology from the overlying site of Koimilot shows differences of degree rather than kind that suggest an elaboration of existing Acheulian tradition. The Koimilot material differs in the production of multiple Levallois flakes per core, smaller (~5–10 cm) flake blanks, and a wider range of Levallois flake shapes obtained by preparatory shaping of the core.

The archaeological site of Koimilot, found south of the Ndau River, overlies upper basaltic tuffs and the Koimilot Tuff, and is the youngest site described here (Fig. 7). Koimilot has an estimated age of ~200,000–250,000 yr on the basis of its position above the Koimilot Tuff and estimates for the termination of Kapthurin Formation sedimentation. Two stratified artifact assemblages were recovered during recent excavations by Tryon (2003, in press(a)) that lack diagnostic shaped or retouched tools, but which are characterized by diverse Levallois methods for the production of flakes of variable sizes and shapes (see Boëda, 1994; Inizan et al., 1999). Levallois flakes and cores, including refitting sets, from the

older strata at Koimilot show the production of small (~5 cm) oval or sub-triangular flakes from centripetally prepared cores by the recurrent and preferential Levallois methods. The overlying stratum shows recurrent Levallois flake production from centripetally prepared cores, as well as large (~10 cm) elongated and triangular preferential Levallois flakes or points, shaped instead by unidirectional or convergent flaking of the core.

The importance of the Koimilot data is twofold. First, the Levallois concept has itself undergone substantial recent revision based on European and Levantine material, with a wide range of flake production strategies now recognized under the term 'Levallois.' The Koimilot Levallois artifacts show variability in a late middle Pleistocene African context comparable to that found at European and Levantine Middle Paleolithic sites (e.g., Boëda et al., 1990) in the methods of core reduction and in the shape and size of the flakes produced. Similar variation has also recently been documented from a limited number of African MSA sites that date to the later Pleistocene (Van Peer, 1998; Wurz, 2002; Pleurdeau, 2003). Recognizing the presence and age of different Levallois systems of flake production found at MSA sites will aid in refining the limits of regional traditions of artifact manufacture (Clark, 1988) and in identifying trajectories of temporal change within the MSA, which presently remain poorly defined (Klein, 1999, 2000).

Sites from within and immediately beneath the Bedded Tuff Member suggest that those elements that characterize the MSA, notably points and Levallois technology, do not appear together as a single package but rather reflect two different, and possibly independent, elements of hominin tool-assisted adaptive strategies, each having its own distinct developmental history (e.g., Boëda, 1991). Our emphasis on typology, specifically the presence or absence of particular forms of tools, cores, or flakes, provides one framework to address change during the Acheulian to Middle Stone Age transition. It forms the foundation for more detailed analyses of changes in lithic assemblage composition and the methods of tool production and core reduction. However, the interstratification of rare tool types and different expressions of Levallois flake production strategies among Acheulian and MSA sites, and even between different MSA strata at Koimilot, suggests that the Acheulian–MSA transition in the Kapthurin Formation was a complex process of change, rather than a sudden replacement 'event.' We recognize that the twofold classification of sites as either Acheulian or MSA based on lithic assemblage composition likely oversimplifies a transition characterized by an incremental or mosaic pattern of change. Technological innovation is additive in nature, resulting in the retention of primitive forms, and this may in part explain the co-occurrence of points and handaxes.

The identity of the hominins responsible for making later middle Pleistocene artifacts is a critical question in understanding the Acheulian–MSA transition because of its broad temporal coincidence with the appearance of *Homo sapiens*. There was probably substantial temporal overlap among early groups of *H. sapiens* and ancestral populations of *H. rhodesiensis* or other species. Which species, or one of several species, made the Kapthurin Formation artifacts is unknown, and rarely can the maker of any Pleistocene archaeological assemblage be identified with certainty. Close relatives in similar environmental settings are expected to share many behavioral features and thus to produce a similar archaeological signature (Lieberman and Shea, 1994). The chronological framework provided by the analysis of Bedded Tuff Member tephra can now be used to integrate the traces of tool production, use, and discard into a broader context of paleoenvironmental variability, in order to explore more fully the archaeological record for the origin of *Homo sapiens*.

Conclusions

Detailed stratigraphic, petrographic and electron microprobe geochemical analysis of the Bedded Tuff Member (K4) allows chronological ordering of archaeological sites within the Kapthurin Formation. This tephrostratigraphic framework provides a highly resolved sequence for examining archaeological change during the later middle Pleistocene. The Bedded Tuff Member (K4) is partitioned into eight subdivisions. The majority of the tephra that compose K4 consist of basaltic and trachytic deposits from a local volcanic source. Basaltic tephra of K4 are subdivided into lower, upper, and evolved basaltic variants on the basis of stratigraphic position and glass and olivine phenocryst chemical composition. The MBTU is a field marker bed, but data presented here show that it is chemically heterogeneous, likely as a result of post-depositional reworking of several formerly discrete layers. A compositional (or 'Daly') gap separates basaltic tephra of the Bedded Tuff Member from stratigraphically overlying locally pumiceous trachytic deposits derived from the same volcanic source. These younger eruptive phases are dated by the $^{40}Ar/^{39}Ar$ method to ~235,000–284,000 yr. Finer grained deposits with siliceous glasses, such as the felsic dust tuffs and the Koimilot Tuff marker bed, suggest a different, more distant source than most of the Bedded Tuff Member succession. These beds provide the foundation for future studies correlating Kapthurin Formation tephra with those from other Pleistocene sedimentary sequences outside of the Baringo basin, extending the time span and geographic scope of our study of hominin behavioral change.

Archaeological sites within the Kapthurin Formation demonstrate the antiquity and complexity of hominin adaptations in the later middle Pleistocene. Point-bearing strata are older than 284,000 yr, and these are interstratified with those containing handaxes and cleavers. Replacement of Acheulian tools by characteristic Middle Stone Age (MSA) implements was neither sudden nor complete. The MSA site of Koimilot shows diverse expressions of Levallois flake production technology in strata dated to ~200,000–250,000 yr. These methods may have developed from existing Acheulian technology. Delimiting the nature and tempo of change that accompanied the appearance of the earliest MSA technology has important implications for models of hominin speciation and dispersal, and provides the archaeological context for the origin of our species (e.g., Foley and Lahr, 1997; Lahr and Foley, 1998). The strength of our

interpretations of evolutionary change and our ability to decipher archaeological complexity must proceed from basic observations of the order of events. We have provided a sound stratigraphic framework for archaeological sites in and immediately beneath the Bedded Tuff Member. Establishing basic chronologies and culture–historical frameworks in the Kapthurin Formation and elsewhere remain vital to our understanding of African prehistory and must precede more elaborate explanations of the evolution of human behavior.

Acknowledgments

Tryon's research was supported by grants from the US National Science Foundation (BCS-0118345), the Wenner-Gren Foundation, the Leakey Foundation, the University of Connecticut Research Foundation, and the Bill Bishop Memorial Trust, with postdoctoral funding from the Fyssen Foundation (Paris) and the Smithsonian Institution (Human Origins Program, National Museum of Natural History). Additional support was provided by grants to McBrearty from the US National Science Foundation (SBR-9601419 and BCS-0217728), from the L.S.B. Leakey Foundation, and the University of Connecticut Research Foundation. Tryon's field research was conducted under research permit MOEST 13/001/30C 229 from the Government of the Republic of Kenya and an exploration and excavation license from the Kenyan Minister for Heritage and Sports, both issued to Tryon. McBrearty has operated under a research permit (OP/13/001/C1391/1) and excavation license issued to Andrew Hill and the Baringo Paleontological Research Project (BPRP), as did Tryon during early stages of the project. We thank Anthony Philpotts, James Eckert, the Archaeology Division of the National Museums of Kenya, Boniface Kimeu, Andrew Hill, and Rhonda Kauffman. We acknowledge Rick Potts, Chris Campisano, Bax R. Barton, and two anonymous reviewers for their challenging yet constructive criticism.

References

Baker, B.H., 1987. Outline of the petrology of the Kenya Rift alkaline province. In: Fitton, J.G., Upton, B.G.J. (Eds.), Alkaline Igneous Rocks. Geological Society Special Publication, vol. 30. Geological Society, London, pp. 293–311.

Barham, L.S., 2000. The Middle Stone Age of Zambia, South-Central Africa. Western Academic and Specialist Press, Bristol, England.

Bishop, W.W., Chapman, G.R., Hill, A., Miller, J.A., 1971. Succession of Cainozoic vertebrate assemblages from the northern Kenya Rift Valley. Nature 233, 389–394.

Boëda, É., 1991. Approche de la variabilité des systèmes de production lithique des industries du paléolithique inférieur et moyen: chronique d'une variabilité attendue. Techniques et Cultures 17–18, 37–79.

Boëda, É., 1994. Le concept Levallois: variabilité des méthodes. Centre National de la Recherche Scientifique Éditions, Paris.

Boëda, É., Geneste, J.-M., Meignen, L., 1990. Identification de chaînes opératoires lithiques du Paléolithique ancien et moyen. Paléo 2, 43–80.

Brown, F.H., 1994. Development of Pliocene and Pleistocene chronology of the Turkana Basin, East Africa, and its relation to other sites. In: Corrucini, R.S., Ciochon, R.L. (Eds.), Integrative Pathways to the Past. Prentice-Hall, Englewood Cliffs, NJ, pp. 285–312.

Brown, F.H., Sarna-Wojcicki, A.M., Meyer, C.E., Haileab, B., 1992. Correlation of Pliocene and Pleistocene tephra layers between the Turkana Basin of East Africa and the Gulf of Aden. Quaternary International 13/14, 55–67.

Cerling, T.E., Brown, F.H., Bowman, J.R., 1985. Low-temperature alteration of volcanic glass: hydration, Na, K, ^{18}O and Ar mobility. Chemical Geology 52, 281–293.

Chapman, G.R., Lippard, S.J., Martyn, J.E., 1978. The stratigraphy and structure of the Kamasia Range, Kenya Rift Valley. Journal of the Geological Society of London 135, 265–281.

Clark, J.D., 1988. The Middle Stone Age of East Africa and the beginnings of regional identity. Journal of World Prehistory 2, 235–305.

Clark, J.D., 1999. Cultural continuity and change in hominid behaviour in Africa during the Middle to Upper Pleistocene transition. In: Ullrich, H. (Ed.), Hominid Evolution: Lifestyles and Survival Strategies. Edition Archaea. Gelsenkirchen/Schwelm, Germany, pp. 277–292.

Clark, J.D., Beyene, Y., WoldeGabriel, G., Hart, W.K., Renne, P., Gilbert, H., Defleur, A., Suwa, G., Katoh, S., Ludwig, K.R., Boisserie, J.-R., Asfaw, B., White, T.D., 2003. Stratigraphic, chronological and behavioural contexts of Pleistocene *Homo sapiens* from Middle Awash, Ethiopia. Nature 423, 747–752.

Cornelissen, E., 1992. Site GnJh-17 and its Implications for the Archaeology of the Middle Kapthurin Formation, Baringo, Kenya. Musée Royale de l'Afrique Centrale, Annales. Sciences Humaines, vol. 133. Musée Royale de l' Afrique Centrale, Tervuren.

Cornelissen, E., 1995. Indications du post-Acheuléen (Sangoen) dans la formation Kapthurin, Baringo, Kenya. L'Anthropologie 99, 55–73.

Cornelissen, E., Boven, A., Dabi, A., Hus, J., Ju Yong, K., Keppens, E., Langhor, R., Moeyersons, J., Pasteels, P., Pieters, M., Uytterschaut, H., van Noten, F., Workineh, H., 1990. The Kapthurin Formation revisited. African Archaeological Review 8, 23–75.

Dagley, P., Mussett, A.E., Palmer, H.C., 1978. Preliminary observations on the palaeomagnetic stratigraphy of the area west of Lake Baringo, Kenya. In: Bishop, W.W. (Ed.), Geological Background to Fossil Man. Scottish Academic Press, Edinburgh, pp. 225–236.

Deino, A., McBrearty, S., 2002. $^{40}Ar/^{39}Ar$ chronology for the Kapthurin Formation, Baringo, Kenya. Journal of Human Evolution 42, 185–210.

Dunkley, P.N., Smith, M., Allen, D.J., Darling, W.G., 1993. The Geothermal Activity and Geology of the Northern Sector of the Kenya Rift Valley. British Geological Survey International Series Research Report SC/93/1, Keyworth, Nottingham.

Feibel, C.S., 1999. Tephrostratigraphy and geological context in paleoanthropology. Evolutionary Anthropology 8, 87–100.

Fisher, R.V., Schmincke, H.-U., 1984. Pyroclastic Rocks. Springer-Verlag, New York.

Foley, R., Lahr, M.M., 1997. Mode 3 technologies and the evolution of modern humans. Cambridge Archaeological Journal 7, 3–36.

Froggatt, P.C., 1992. Standardization of the chemical analysis of tephra deposits. Report of the ICCT Working Group. Quaternary International 13/14, 93–96.

Gibbard, P.L., 2003. Definition of the Middle-Upper Pleistocene boundary. Global and Planetary Change 36, 201–208.

Grayson, D.K., Cole, S.C., 1998. Stone tool assemblage richness during the Middle and Early Upper Paleolithic in France. Journal of Archaeological Science 25, 927–938.

Henshilwood, C.S., Marean, C.W., 2003. The origin of modern human behavior: critique of the models and their test implications. Current Anthropology 44, 627–651.

Hill, A., Curtis, G., Drake, R., 1986. Sedimentary stratigraphy of the Tugen Hills, Baringo District, Kenya. In: Frostick, L.E., Renaut, R.W., Reid, I., Tiercelin, J.-J. (Eds.), Sedimentation in the African Rifts. Geological Society of London Special Publication, vol. 25. Blackwell, Oxford, pp. 285–295.

Howell, F.C., 1999. Paleo-demes, species clades, and extinctions in the Pleistocene hominin record. Journal of Anthropological Research 55, 191–243.

Inizan, M.-L., Reduron-Ballinger, M., Roche, H., Tixier, J., 1999. Technology and Terminology of Knapped Stone. CREP, Nanterre.

Isaac, G.L., 1975. Sorting out the muddle in the middle: an anthropologist's post-conference appraisal. In: Butzer, K.W., Isaac, G.L. (Eds.), After the Australopithecines: Stratigraphy, Ecology, and Culture Change in the Middle Pleistocene. Mouton Publishers, The Hague, pp. 875–887.

Klein, R.G., 1999. The Human Career: Human Biological and Cultural Origins. Chicago Univ. Press, Chicago.

Klein, R.G., 2000. Archaeology and the evolution of human behavior. Evolutionary Anthropology 9, 17–36.

Lahr, M.M., Foley, R., 1998. Towards a theory of modern human origins: geography, demography, and diversity in recent human evolution. Yearbook of Physical Anthropology 41, 137–176.

Le Gall, B., Tiercelin, J.-J., Richert, J.-P., Gente, P., Sturchio, N.C., Stead, D., Le Turdu, C., 2000. A morphotectonic study of an extensional fault zone in a magma-rich rift: the Baringo Trachyte Fault System, central Kenya Rift. Tectonophysics 320, 87–106.

Leakey, M., Tobias, P.V., Martyn, J.E., Leakey, R.E.F., 1969. An Acheulian industry with prepared core technique and the discovery of a contemporary hominid mandible at Lake Baringo, Kenya. Proceedings of the Prehistoric Society 3, 48–76.

Lieberman, D., Shea, J.J., 1994. Behavioral differences between archaic and modern humans in the Levantine Mousterian. American Anthropologist 96, 300–332.

Macdonald, R., 1987. Quaternary peralkaline silicic rocks and caldera volcanoes of Kenya. In: Fitton, J.G., Upton, B.G.J. (Eds.), Alkaline Igneous Rocks. Geological Society Special Publication, vol. 30. Geological Society, London, pp. 313–333.

Martyn, J., 1969. The Geologic History of the Country Between Lake Baringo and the Kerio River, Baringo District Kenya. Unpublished Ph.D. dissertation, University of London.

McBirney, A.R., 1984. Igneous Petrology. Freeman, Cooper and Co., San Francisco.

McBrearty, S., 1999. Archaeology of the Kapthurin Formation. In: Andrews, P., Banham, P. (Eds.), Late Cenozoic Environments and Hominid Evolution: A Tribute to Bill Bishop. Geological Society, London, pp. 143–156.

McBrearty, S., 2001. The Middle Pleistocene of East Africa. In: Barham, L.H., Robson-Brown, K. (Eds.), Human Roots: Africa and Asia in the Middle Pleistocene. Western Academic and Specialist Press, Limited, Bristol, UK, pp. 81–97.

McBrearty, S., Brooks, A., 2000. The revolution that wasn't: a new interpretation of the origin of modern human behavior. Journal of Human Evolution 39, 453–563.

McBrearty, S., Tryon, C.A., 2006. From Acheulian to Middle Stone Age in the Kapthurin Formation of Kenya. In: Hovers, E., Kuhn, S.L. (Eds.), Transitions Before the Transition: Temporal Trends in the Middle Paleolithic and Middle Stone Age. Springer, New York, pp. 257–277.

McBrearty, S., Bishop, L.C., Kingston, J.D., 1996. Variability in traces of Middle Pleistocene hominid behavior in the Kapthurin Formation, Baringo, Kenya. Journal of Human Evolution 30, 563–580.

McDougall, I., Brown, F.H., Fleagle, J.G., 2005. Stratigraphic placement and age of modern humans from Kibish, Ethiopia. Nature 433, 733–736.

Nelson, C.M., 1993. A standardized site enumeration system for the continent of Africa. Nyame Akuma 40, 62–67.

Orton, G.J., 1996. Volcanic environments, In: Reading, H.G. (Ed.), Sedimentary Environments: Processes, Facies and Stratigraphy, third ed. Blackwell Science, London, pp. 485–567.

Philpotts, A.R., 1990. Principles of Igneous and Metamorphic Petrology. Prentice Hall, Englewood Cliffs, NJ.

Pleurdeau, D., 2003. Le Middle Stone Age de la grotte du Porc-Épic (Dire Dawa, Éthiopie): gestion des matières premières et comportements techniques. L'Anthropologie 107, 15–48.

Potts, R., Behrensmeyer, A.K., Ditchfield, P., 1999. Paleolandscape variation and Early Pleistocene hominid activities: members 1 and 7, Olorgesailie Formation, Kenya. Journal of Human Evolution 37, 747–788.

Reed, S.J.B., 1996. Electron Microprobe Analysis and Scanning Electron Microscopy in Geology. Cambridge Univ. Press, Cambridge.

Renaut, R.W., Owen, R.B., 1980. Late Quaternary fluvio-lacustrine sedimentation and lake levels in the Baringo Basin, northern Kenya Rift Valley. Recherches Gologiques en Afrique 5, 130–133.

Sarna-Wojcicki, A.M., Davis, J.O., 1991. Quaternary tephrochronology. In: Morrison, R.B. (Ed.), The Geology of North America: Quaternary Nonglacial Geology; Coterminous United States. Geological Society of America, Boulder, CO, pp. 93–116.

Sarna-Wojcicki, A.M., Pringle, M.S., Wijbrans, J., 2000. New $^{40}Ar/^{39}Ar$ age of the Bishop Tuff from multiple sites and sediment rate calibration for the Matuyama–Brunhes boundary. Journal of Geophysical Research 105 (B9), 21431–21443.

Schmid, R., 1981. Descriptive nomenclature of classification of pyroclastic deposits and fragments: recommendations of the IUGS subcommission on the systematics of igneous rocks. Geology 9, 41–43.

Singer, B.S., Relle, M.K., Hoffman, K.A., Battle, A., Laj, C., Guillou, H., Carracedo, J.C., 2002. Ar/Ar ages from transitionally magnetized lavas on La Palma, Canary Islands, and the geomagnetic instability timescale. Journal of Geophysical Research 107 (B11), 2307.

Smith, G.A., 1991. Facies sequences and geometries in continental volcaniclastic sequences. In: Fisher, R.V., Smith, G.A. (Eds.), Sedimentation in Volcanic Settings. Society for Sedimentary Geology Special Publication, vol. 45. Society of Sedimentary Geology, Tulsa, pp. 109–122.

Stringer, C., 2002. Modern human origins: progress and prospects. Philosophical Transactions of the Royal Society of London, Series B: Biological Sciences 357, 563–579.

Tallon, P.W.J., 1976. The Stratigraphy, Palaeoenvironments and Geomorphology of the Pleistocene Kapthurin Formation, Kenya. Unpublished Ph.D. dissertation, Queen Mary College.

Tallon, P.W.J., 1978. Geological setting of the hominid fossils and Acheulian artifacts from the Kapthurin Formation, Baringo District, Kenya. In: Bishop, W.W. (Ed.), Geological Background to Fossil Man. Scottish Academic Press, Edinburgh, pp. 361–373.

Tiercelin, J.-J., Vincens, A., Barton, C., Carbonel, P., Casanova, J., Delibrias, G., Gasse, F., Grosdidier, E., Herbin, J.-P., Huc, A.Y., Jardiné, S., Le Fournier, J., Méliéres, F., Owen, R.B., Page, P., Palacios, C., Paquet, H., Péniguel, G., Peypouquet, J., Raynaud, J., Renaut, R.W., De Renéville, P., Richert, J.-P., Riff, R., Robert, P., Seyve, C., Vandenbroucke, M., Vidal, G., 1987. Le demi-graben de Baringo-Bogoria, Rift Gregory, Kenya. 30,000 ans d'histoire hydrologique et sédimentaire. Bulletin de Centres Recherche Exploration-Production (Elf Aquitaine), vol. 11, pp. 249–540.

Tishkoff, S.A., Williams, S.M., 2002. Genetic analysis of African populations: human evolution and complex disease. Nature Reviews. Genetics 3, 611–621.

Tryon, C.A., 2002. Middle Pleistocene sites from the "southern" Kapthurin Formation of Kenya. Nyame Akuma 57, 6–13.

Tryon, C.A., 2003. The Acheulian to Middle Stone Age Transition: Tephrostratigraphic Context for Archaeological Change in the Kapthurin Formation, Kenya. Unpublished Ph.D., University of Connecticut.

Tryon, C.A., in press(a). 'Early' Middle Stone Age lithic technology of the Kapthurin Formation (Kenya). Current Anthropology.

Tryon, C.A., in press(b). Le concept Levallois en Afrique. Annales Fyssen.

Tryon, C.A., McBrearty, S., 2002. Tephrostratigraphy and the Acheulian to Middle Stone Age transition in the Kapthurin Formation, Baringo, Kenya. Journal of Human Evolution 42, 211–235.

Tryon, C.A., McBrearty, S., Texier, P.-J., in press. Levallois lithic technology from the Kapthurin Formation, Kenya: Acheulian origin and Middle Stone Age diversity. African Archaeological Review.

Van Peer, P., 1998. The Nile Corridor and the Out-of-Africa model: an examination of the archaeological record. Current Anthropology 39, S115–S140.

Van Peer, P., Fullagar, R., Stokes, S., Bailey, R.M., Moeyersons, J., Steenhudt, F., Geerts, A., Vanderbeken, T., De Dapper, M., Geus, F., 2003. The Early to Middle Stone Age transition and the emergence of modern human behavior at site 8-B-11, Sai Island, Sudan. Journal of Human Evolution 45, 187–194.

White, T.D., Asfaw, B., DeGusta, D., Gilbert, H., Richards, G.D., Suwa, G., Howell, F.C., 2003. Pleistocene Homo sapiens from Middle Awash, Ethiopia. Nature 423, 742–747.

Wurz, S., 2002. Variability in the Middle Stone Age lithic sequence, 115,000–60,000 years ago at Klasies River, South Africa. Journal of Archaeological Science 29, 1001–1015.

Yamei, H., Potts, R., Baoyin, Y., Zhengtang, G., Deino, A., Wei, W., Clark, J., Guangmao, X., Weiwen, H., 2000. Mid-Pleistocene Acheulean-like stone technology of the Bose basin, South China. Science 287, 1622–1626.